

## Accepted Manuscript

Title: A study of ethanol dehydrogenation to acetaldehyde over copper/zinc aluminate catalysts

Authors: Gabriella Garbarino, Paola Riani, María Villa García, Elisabetta Finocchio, Vicente Sanchez Escribano, Guido Busca



PII: S0920-5861(18)31364-6  
DOI: <https://doi.org/10.1016/j.cattod.2019.01.002>  
Reference: CATTOD 11873

To appear in: *Catalysis Today*

Received date: 11 August 2018  
Revised date: 16 December 2018  
Accepted date: 2 January 2019

Please cite this article as: Garbarino G, Riani P, Villa García M, Finocchio E, Escribano VS, Busca G, A study of ethanol dehydrogenation to acetaldehyde over copper/zinc aluminate catalysts, *Catalysis Today* (2019), <https://doi.org/10.1016/j.cattod.2019.01.002>

This is a PDF file of an unedited manuscript that has been accepted for publication. As a service to our customers we are providing this early version of the manuscript. The manuscript will undergo copyediting, typesetting, and review of the resulting proof before it is published in its final form. Please note that during the production process errors may be discovered which could affect the content, and all legal disclaimers that apply to the journal pertain.

## A study of ethanol dehydrogenation to acetaldehyde over copper/zinc aluminate catalysts.

Gabriella Garbarino<sup>1,2</sup>, Paola Riani<sup>2,3</sup>, María Villa García<sup>4</sup>, Elisabetta Finocchio<sup>1,2</sup>, Vicente Sanchez Escribano<sup>4</sup> and Guido Busca<sup>1,2\*</sup>

<sup>1</sup> Università degli Studi di Genova, Dipartimento di Ingegneria Civile, Chimica e Ambientale (DICCA), Laboratorio di chimica delle superfici e catalisi, Via all'Opera Pia 15, 16145, Genova, Italy

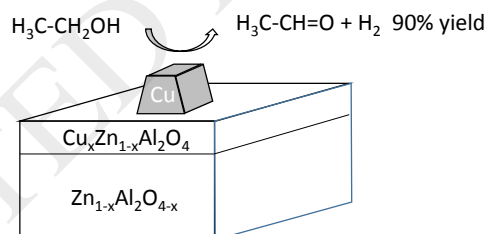
<sup>2</sup> Consorzio INSTM UdR di Genova, via Dodecaneso 31, 16146 Genova, Italy

<sup>3</sup> Università degli Studi di Genova, Dipartimento di Farmacia (DIFAR), Viale Cembrano 4 16148 Genova, Italy

<sup>4</sup> Departamento de Química Inorgánica, Universidad de Salamanca, Pl. de la Merced s/n, 37008 Salamanca, Spain

\*Corresponding author: e-mail [guido.busca@unige.it](mailto:guido.busca@unige.it). Tel. +390103536024 FAX +390103532586

Graphical abstract



### Highlights

- Cu/ZnAl<sub>2</sub>O<sub>4</sub> catalysts were prepared by impregnation of commercial ZnAl<sub>2</sub>O<sub>4</sub>
- The 19.3 % wt Cu/ZnAl<sub>2</sub>O<sub>4</sub> allows 90% yield at 673 K, with 100% conversion.

- The catalysts reduce and condition themselves on stream by reacting with ethanol.
- Copper particles over Zn-poor  $Zn_xAl_2O_{3+x}$  spinel particles are the most active.
- IR spectra show the intermediacy of Cu-bonded surface ethoxy-groups.

Abstract. Catalysts composed of copper supported on  $ZnAl_2O_4$  were prepared by conventional impregnation of a commercial zinc aluminate powder using copper nitrate water solutions. The fresh catalysts were characterized by XRD, skeletal IR and DR-UV-Vis spectroscopies, FE-SEM microscopy, BET and pore volume measurements. The catalysts were tested in the conversion of ethanol (96% assay, 6.9 % vol in nitrogen) at GHSV 10000  $h^{-1}$ . The spent catalysts were characterized by FESEM and DR-UV-Vis.

These catalysts are very efficient for the dehydrogenation of ethanol to acetaldehyde, with selectivities in excess of 95 % at low conversion, persisting also at total conversion, allowing yields up to 90 %. The most active species appear to be on copper metal nanoparticles grown over Zn-poor substoichiometric spinel nanoparticles. The catalysts reduce themselves on stream. The high selectivity at low temperature is in part due to the ability of copper to kill the dehydration activity to diethyl ether. The selectivity to acetaldehyde decreases at very high temperature ( $> 673$  K) due to overconversion of acetaldehyde to thermodynamically more stable products such as methane, acetone, propene and carbon oxides, as well as to increased competition with the more favored dehydration reaction. IR studies show the intermediate role of surface ethoxy-groups.

Keywords: Ethanol conversion; acetaldehyde manufacture; copper catalysts; Zinc aluminate support; thermodynamics.

## 1. Introduction.

In the near future, industrial organic chemistry must shift from fossil raw materials to renewable raw materials, in order to attain sustainability. A number of organic molecules directly coming from renewable raw materials will become key platform chemicals for the production of monomers and secondary intermediates. It is consequently urgent to shift research efforts to investigate the production and the conversion of such platform molecules as well as to develop new processes based on their transformation. A good example of this innovative eco-friendly research approach was given in recent years by the group led by Maria Ziolek at the University of Poznan (Poland), who deeply investigated the industrial chemistry of glycerol, an intermediate coming from the chemistry of triglycerides, developing new catalysts for its selective oxidation [1,2], esterification [3] and acetalization [4], as well as for the synthesis of nitriles from it [5].

Ethanol produced by fermentation of lignocellulosics is also expected to become a primary intermediate in the new industrial organic chemistry based on renewables [6,7]. Among the secondary intermediates potentially obtainable by converting (bio)ethanol, (bio)acetaldehyde may play a relevant role in the future. In fact, according to Sun, acetaldehyde is the main intermediate for the production of several secondary intermediates [8].

Nowadays, acetaldehyde is mainly manufactured as a petrochemical intermediate with the Wacker-Hoechst process by ethylene oxidation in the liquid phase in the presence of Cu-Pd chloride homogeneous catalysts [9]. Its production was significantly contracted starting from the ninetens when the acetic acid manufacture by acetaldehyde oxidation processes were progressively substituted by the more performant methanol carbonylation processes, based on syngas produced by natural gas steam reforming.

However, in very recent years, acetaldehyde world production is increasing again and it is projected to exceed 1.4 million tons by 2022 [10]. Acetaldehyde is widely applied in food engineering as a preservative and a flavouring agent. It is also a main chemical platform to produce a number of relevant chemicals such as pyridines (for agricultural chemicals), ethylacetate, other acetate esters and pentaerythritol for coatings industry, 1,3 butylene glycol for polymers, crotonaldehyde, glyoxal, etc..

Bio-acetaldehyde can be produced as a renewable intermediate either by dehydrogenation or by partial oxidation of bioethanol. Ethanol dehydrogenation processes were performed in the past at 533-563 K, over copper chromite catalysts with low conversion (25-50 %) and recycle of the unconverted ethanol [8,11,12]. The final acetaldehyde yield was ca. 90 % with coproduction of several byproducts such as butyric acid, crotonaldehyde, and ethyl acetate, due to limited selectivity to the target product.

In recent years, ethanol dehydrogenation is object of renewed interest: very selective catalysts have been developed [13,14,15]. Also in this case, however, selectivity drops at high conversion.

Supported copper catalysts are largely applied as catalysts for dehydrogenation of alcohols to carbonyl compounds, such as Cu-ZnO, Cu-SiO<sub>2</sub>, Cu-Al<sub>2</sub>O<sub>3</sub>, Cu-ZnO-Al<sub>2</sub>O<sub>3</sub> [16,17,18,19,20]. In particular, the Cu-ZnO-Al<sub>2</sub>O<sub>3</sub> system is a very relevant one in industrial catalysis being the basic composition of catalysts for methanol synthesis [21], low temperature water gas shift [22], methanol decomposition and its steam reforming [23],

hydrogenation of ketones to alcohols [24] and, as said, dehydrogenation of alcohols to ketones and aldehydes [25].

Following our previous research on ethanol conversion over different catalysts [26-31], we report here our data on the conversion of ethanol to acetaldehyde over Cu-ZnAl<sub>2</sub>O<sub>4</sub> catalysts. Besides the interest for the ethanol to acetaldehyde process, this research is also of interest in relation to the attempt to manufacture from (bio)ethanol other compounds such as acetic acid [32], ethylacetate [33], acetone [27], 1-butanol [34], butadiene [35,36], isobutene [37], by single step processes. In fact, acetaldehyde may be supposed to be a primary intermediate in these processes.

## 2. Experimental.

### 2.1 Materials

In Table 1, a summary of data on the catalytic materials used here is reported. The support used is a commercial Zinc aluminate (Puralox Zn44) manufactured by Sasol (44 wt% and 56 wt% of ZnO and alumina respectively with a surface area of 104 m<sup>2</sup>/g ). Copper was supported by conventional wet impregnation method, using Cu(NO<sub>3</sub>)<sub>2</sub>\*3H<sub>2</sub>O solution. The samples have been dried for 5 h at 363 K under magnetic stirring and then have been calcined in static air at 773 K for 5 hours. The notation adopted is ZA for the bare support and C<sub>x</sub>ZA for Cu-based catalysts, with x=10, 30 and 50 accrosint to the formula  $x = \text{wt}_{\text{CuO}} * 100 / \text{wt}_{\text{ZnAl}_2\text{O}_4}$

### 2.2 Materials characterisation.

XRD measure was performed on a Siemens D-500 diffractometer (CuK $\alpha$  radiation, Ni filter; operated in the vertical mode on 40 kV and 30 mA) equipped with the Diffract AT V3 software package. The patterns were recorded over the 2 $\theta$  angle ranging from 10° to 80° at a scan rate of 1.5 degree/min.

BET surface area and porosity were measured using N<sub>2</sub> adsorption/desorption at 77 K determined volumetrically with a Micromeritics Gemini 2390a instrument. The sample has been previously outgassed at 383 K for 2 hours in N<sub>2</sub>.

ICP-OES analysis have been performed with a plasma emission spectrometer model Ultima II de Yobin Ivon. Samples for elemental analysis were obtained by treatment of 0.1 g of sample in HNO<sub>3</sub> + HCl + HF concentrated acid solution in a high pressure reactor.

DR-UV-vis-NIR spectra of both fresh and spent catalysts were collected with a JASCO V570 instrument equipped with an integrating sphere.

Sample morphology was observed by means of a Scanning Electron Microscope Zeiss SUPRA 40 VP microscope, provided with a field emission gun as emitter (FE-SEM). This instrument is equipped with a solid state detector for backscattered electrons, with a high sensitivity "InLens" secondary electron detector and with a EDX microanalysis OXFORD "INCA Energie 450x3". Sample powders were directly mounted on a high purity conductive double sided adhesive carbon tabs, and the specimen so obtained was then imaged.

FT-IR spectra were recorded on a Nexus ThermoNicolet instrument (OMNIC software, DTGS detector, 100 scans). For skeletal studies, the samples were pressed into thin wafers with KBr and spectra were recorded in air. FT-IR studies of ethanol conversion were performed on compacted powder disks of 15-30 mg activated in vacuum at 773 K before adsorption experiments. Ethanol (several Torr) was adsorbed at RT and spectra were recorded in the presence of the gas and at increasing temperature (473-773 K).

### 2.3 Catalytic activity measures

Catalytic experiments were performed at atmospheric pressure in a tubular flow reactor (i.d. 7 mm) using 0.5 g of catalyst, 60-70 mesh sieved, thus achieving a ratio between the particle and internal reactor diameter near 25). Ethanol (96% assay, from Sigma Aldrich) was kept with a concentration of 6.9 % vol in nitrogen. The total flow rate has been set at 80 cc/min, corresponding to a GHSV of 10000 h<sup>-1</sup>. The carrier gas (nitrogen) was passed through a bubbler containing ethanol maintained at constant temperature (298 K) in order to obtain the desired partial pressures. The temperature in the experiment was varied stepwise from 423 K to 773 K.

The outlet gases were analyzed by a gas chromatograph (GC) Agilent 4890 equipped with a Varian capillary column "Molsieve 5A/Porabond Q Tandem" and TCD and FID detectors in series. In order to identify the compounds of the outlet gases, a GC-MS Thermo Scientific with TG-SQC column (30 m x 0.25 mm x 0.25 μm) was used.

Ethanol conversion is defined as usual:

$$X_{\text{EtOH}} = (n_{\text{EtOH(in)}} - n_{\text{EtOH(out)}}) / n_{\text{EtOH(in)}}$$

while selectivity to product *i* is defined as follows:

$$S_i = n_i / (v_i (n_{\text{EtOH(in)}} - n_{\text{EtOH(out)}}))$$

where  $n_i$  is the moles number of compound  $i$ , and  $v_i$  is the ratio of stoichiometric reaction coefficients.

### 3. Results.

#### 3.1. Bulk and morphological catalyst characterization.

In table 1, analytical data on Cu content coming from nominal composition data and ICP-OES analyses over the all sample are reported. The measured copper amount corresponds quite well with the nominal one. EDX composition is also in good agreement with ICP-OES data (thus it has been not reported). In the Cu10ZA sample, the amount of copper is lower than that expected for a geometrical coverage of the support surface, with nearly  $12 \text{ \AA}^2$  of support surface available for every Cu atom or Cu-O couple. In the case of Cu30ZA and Cu50ZA samples, instead, the coverage is higher than that needed to cover the entire surface of the support. BET surface area is progressively reduced from 95 to  $60 \text{ m}^2/\text{g}$  by increasing copper content. However, the surface areas measured per weight of support is nearly constant at  $90 \text{ m}^2/\text{g}$ , suggesting that the morphology of the catalysts essentially does not change. The nitrogen adsorption/desorption isotherms (Fig. 1, left) correspond to the type IV of the IUPAC classification, characteristics of mesoporous materials, with a pore width higher than 4nm. The hysteresis loop is intermediate in between H1 and H2 [38] where pore structure is complex and in some way affected by network effects. A monomodal pore size distribution is observed (Fig. 1, right) with pore diameters ranging in-between 4 and 9 nm, centered near 7 nm. The measured pore volume for the bare  $\text{ZnAl}_2\text{O}_4$  support is  $140 \text{ cm}^3_{\text{STP}}/\text{g}$  corresponding to  $0.217 \text{ cm}^3/\text{g}$  considering liquid nitrogen. The copper containing samples present a similar predominant morphology with a progressive decrease of the pore volume to  $0.139 \text{ cm}^3/\text{g}$  by increasing copper oxide content up to 28.5 wt% (Cu50ZA). While the maximum in the pore size distribution curve is constant with Cu content at 7 nm, an erosion is clearly found on the low size side of the curve, showing that the smallest size pores (3-6 nm) tend to disappear.

XRD patterns (Figure 2) show the features of the cubic spinel  $\text{ZnAl}_2\text{O}_4$  (JCPDS No. 05-0669) in all cases. The patterns of the copper containing samples also contain the features of the CuO (tenorite, JCPDS No. 05-0661) phase, increasing in intensity by increasing copper content. The average crystallite size of the CuO phase evaluated with Scherrer equation on the peak at  $2\theta=37.8^\circ$  is 16, 18 and 20 nm for Cu10ZA, Cu30ZA and

Cu50ZA. Thus, even if copper species could be geometrically fully dispersed in the Cu10ZA sample, also in this case CuO particles exist. From an analysis of the intensities of the XRD peaks (see right section of Fig. 2) we note that the peaks of the spinel phase decrease with the ratio 1:0.95:0.79:0.53, values in slight excess with respect to the nominal ratios 1:0.90:0.70:0.50. The trend of the intensities of the peaks of CuO for the copper containing samples is around 1: 4.7: 6.2, with respect to the 1:3:5 nominal content. From these intensity data we can calculate that nearly 50% of the Cu content in Cu10ZA is dispersed on the support surface in an XRD undetectable form, while 50% is in the form of CuO. This suggests that dispersion of copper species in an XRD undetectable form is “selective” and involves nearly 1 Cu atom per 20 Å<sup>2</sup>. The additional amount of Cu deposited on Cu30ZA may be entirely in the form of additional CuO. On the other hand in the case of Cu50ZA part of additional Cu species should enter the spinel phase maybe forming cation excess spinel phases.

The FE-SE micrographs (Fig. 3) show that the support has a primary particle size lower than 20 nm, in part agglomerated in larger secondary particles. FE-SEM/EDX data on single particles show that in the support, few particles very rich in Zn exist together with several particles whose composition is Zn-poor with respect to the nominal spinel stoichiometry. The latter are likely constituted by cation deficient spinel structure  $Zn_xAl_2O_{3+x}$ , with  $x < 1$ .

The FE-SEM image of the sieved fraction (size > 60-70 mesh) is reported in Figure 3 together with those of the Cu-containing samples. The FE-SEM/EDX data of the sample Cu10ZA show that the copper amount in the entire powder is measured about 9 %, respecting the nominal composition. However, it has to be remarked that most support particles show moderate brightness and a Cu content of  $\approx 4$  wt%, while additionally, bright particles are also present with very high CuO concentration (up to 90 wt% as CuO, up to 60 wt% as Cu). Interestingly, most of these Cu-rich particles show a Zn/Al atomic ratio lower than 0.5. Thus, it is evident that deposition of copper is inhomogeneous and, in some way, “selective”. This suggests that copper rich particles form in contact with stoichiometric deficient spinel particles, with composition  $Zn_xAl_2O_{3+x}$ , with  $x < 1$ . It is possible that contact of copper is favored over these non-stoichiometric spinel structure, first forming stoichiometric spinels with composition  $Cu_{1-x}Zn_xAl_2O_4$ , over which nucleation of CuO is favored. It seems that on nearly stoichiometric spinel particles, with composition  $ZnAl_2O_4$ , copper tends to disperse homogeneously as a “surface monolayer”. This also occurs for samples Cu30ZA and Cu50ZA, where the number and maybe the size of the Cu-rich

particles increase progressively. The FE-SEM data agree with XRD showing the presence of unsupported CuO particles together with dispersed Cu(II) on the support in all cases.

The skeletal IR spectrum (Fig. 4) of the support ZA agrees well with that reported for the spinel  $\text{ZnAl}_2\text{O}_4$  [39,40,41] as well as for  $\text{Cu}_{1-x}\text{Zn}_x\text{Al}_2\text{O}_4$  spinels [42], with three IR active fundamentals found at 686, 555 and 497  $\text{cm}^{-1}$ , the fourth IR active fundamental being expected near 225  $\text{cm}^{-1}$ , i.e. out of the range of our measurement. The addition of copper causes the modification of the spectrum, with the absorption increasing in the range around 500  $\text{cm}^{-1}$ , where in fact the complex spectrum of CuO (tenorite) [43,44] is observed.

The DR-UV spectrum of the support ZA (Fig. 5) shows a main maximum at 245 nm and a shoulder near 325 nm. The position of the main band (5.06 eV) corresponds closely to that reported by other authors for  $\text{ZnAl}_2\text{O}_4$  nanoparticles [45], while the weak absorption at 3.8 eV is due either to ZnO rich particles or to larger bulk  $\text{ZnAl}_2\text{O}_4$  particles [46].

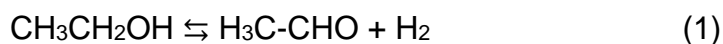
The UV-Vis spectra of the copper-containing samples (Fig. 5) show a strong sharp absorption centered near 250 nm together with a weak and broad one at 720 nm. The former has its maximum intensity in sample Cu10ZA and slightly decreases in intensity for samples more charged in copper. The latter absorption grows strongly in intensity from Cu10ZA to Cu30ZA, while is only slightly more intense for sample Cu50ZA with respect to sample Cu30ZA. The higher wavelength limit of this absorption closely corresponds to the edge of the absorption found in the spectrum of CuO, tenorite, with the absorption onset at 900 nm (1.38 eV), in agreement also with literature data [47,48]. The spectra of our fresh catalysts might be due to the superimposition of the absorption edge due to CuO nanoparticles with the absorption bands due to dispersed  $\text{Cu}^{2+}$  ions, i.e. the strongest band at 250 nm, due to the  $\text{O}^{2-} \rightarrow \text{Cu}^{2+}$  ligand-to-metal charge transfer transition and the band centered at ca 720 nm due to spin allowed  $2E_g / 2T_{2g} d \rightarrow d$  transition of  $\text{Cu}^{2+}$  ion in pseudo-octahedral coordination [49].

### 3.2 Ethanol conversion to acetaldehyde: thermodynamics and blank experiments.

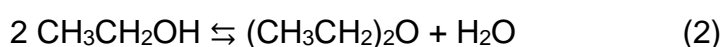
Thermal conversion of ethanol has been studied without catalyst in the IR cell, and with a bed of low surface area silica glass (supposed to be catalytically inactive) in the flow reactor. In the IR cell a very limited conversion of ethanol was found at 673 K producing acetaldehyde with traces of ethylene, while at 773 K acetaldehyde, ethylene, methane and CO are observed, together with largely predominant unconverted ethanol. A similar result has been

observed in the flow reactor, where zero conversion was found at 623 K and below, with production of small amounts of acetaldehyde and ethylene at higher temperatures.

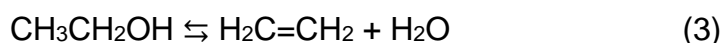
According to thermodynamic calculations (Fig. 6), the equilibrium of the dehydrogenation reaction of ethanol to acetaldehyde



in our feed conditions is increasingly favored at increasing temperature. Conversion of ethanol should be significant (> 75%) at 550 K, with nearly full yield of acetaldehyde above 700 K. However, dehydration to diethyl ether (at lower temperature)



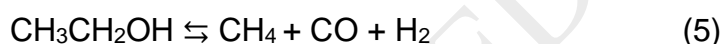
and to ethylene (at higher temperature)



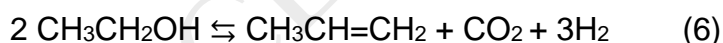
is by far more favored than dehydrogenation in all the investigated temperature range. Here we show that acetaldehyde is also unstable with respect to decomposition (decarbonylation) to methane and CO



Which corresponds to the decomposition of ethanol to CH<sub>4</sub>, CO and H<sub>2</sub>



On the other hand, calculations show that acetaldehyde is also unstable with respect to a number of other reactions such as those producing acetone and propene. In Fig. 6,d the reaction producing propylene



has also been considered.

According to these data we can conclude that the thermal reaction (without catalyst) is in our conditions kinetically hindered until 700 K, being ethanol conversion very limited, and that only dehydration to ethylene and decomposition to CH<sub>4</sub>+CO are observed in our non-catalytic experiments.

### 3.3. Catalytic activity in the flow reactor.

In Figure 7, the data concerning the catalytic activity of the ZA catalyst in the conversion of ethanol are reported. The conversion of ethanol is significant at 573 K and above, approaching totality at 773 K. At low temperature and conversion, diethyl ether is the main product with selectivity of near 57 %, with coproduction of acetaldehyde (29 % selectivity), ethylacetate (7 % selectivity) and ethylene (5 % selectivity). This behavior provides evidence of the coexistence on ZA of dehydration activity (to diethyl ether and ethylene) with dehydrogenation activity, producing acetaldehyde and, with a complex reaction path, likely also ethylacetate. By increasing the reaction temperature, diethyl ether selectivity decreases, while acetaldehyde selectivity goes through a maximum, 55 % at 723 K. However, the yield to acetaldehyde reaches a maximum at 43 % at 723 K decreasing to 36 % at 773 K. Ethylene selectivity grows slowly to 12 % at 773 K while ethylacetate selectivity also does not overpass 11 % and declines too at 773 K. At this temperature several other compounds form with selectivities < 8 % each (propylene, acetone, CO<sub>2</sub>, butenes, benzene, pentanone).

In Figure 8, the results of the same experiment performed with the Cu10ZA catalyst are reported. The conversion of ethanol over the Cu10ZA catalyst is slightly lower with respect to that observed over the bare support ZA, at any temperature. In particular, no activity is found at 573 K while conversion of ethanol at 773 K achieves 80%. On the other hand, a completely different selectivity pattern is observed: selectivity to acetaldehyde is always very high, declining from 96% to 92 % by increasing temperature, with the co-presence of ethylacetate (around 5% selectivity) and very small amounts of n-butanal. The behavior shows that copper species, in spite of being far less than that needed to cover the entire support surface, entirely poisoned the acid-base sites of the support [32] active in producing diethyl ether. It seems likely that copper species dispersing on the support as well as CuO growing on the support poison and neutralize specifically its acid sites, thus deactivating the dehydrogenation activity of the support. The experiment was stopped at 773 K to not overpass the calcination temperature of the sample.

In Figure 9, the data of the same experiment performed over the 30CuZA catalyst are reported. This catalyst is definitely more active than the previous one, with very small conversion found already at 473 K and 33% conversion at 523 K and 100 % conversion at 673 K. Also this catalyst gives rise to very high selectivity to acetaldehyde which declines slightly from 96% at 523 K to 90 % at 673 K. Acetaldehyde yield is 89% at 623 K and 90 % at 673 K. In these conditions, the thermodynamic equilibrium for dehydrogenation reaction

is nearly approached. At higher temperature selectivity to acetaldehyde declines progressively with increasing of yield acetone and CO<sub>2</sub> and, intermediately, of propene, but also with the reappearance of the dehydration products diethyleter and ethylene.

In Figure 10, the catalytic behavior of Cu50ZA in the same conditions is reported. The Cu50ZA catalyst is less active than the Cu30 catalyst with only 12 % conversion at 573 K and approaching full conversion only at 773 K. Also this catalyst shows very high selectivity to acetaldehyde, in the range 95-90% producing 87 % acetaldehyde yield at 773 K.

### 3.3. *Ethanol conversion in the IR cell.*

The conversion of ethanol has been investigated on the Cu10ZA catalyst using IR spectroscopy. This is the only Cu-containing sample that transmits IR light even during reaction. The analysis of the gas phase (Figure 11) spectra show that gas-phase acetaldehyde (rotovibrational C=O stretching at 1746 cm<sup>-1</sup> and C-H stretching at 2715 cm<sup>-1</sup>) starts to be detectable at 473 K, while ethylacetate appears (rotovibrational C=O stretching at 1764 cm<sup>-1</sup> visible as a shoulder on the νCO band of acetaldehyde). It is evident, even if weak, starting from 523 K. At the same temperature also traces of diethyl ether are observed (rotovibrational C-O-C asymmetric stretching at 1116 cm<sup>-1</sup>). Methane (sharp peaks at 3016 cm<sup>-1</sup> and 1304 cm<sup>-1</sup>, CH<sub>4</sub> stretching and deformation), CO (νCO band at 2140 cm<sup>-1</sup>), ethylene (CH<sub>2</sub> wagging at 949 cm<sup>-1</sup>), propylene (CH<sub>2</sub> wagging at 912 cm<sup>-1</sup>) and acetone (C=O stretching at 1741 cm<sup>-1</sup> and C-C-C asymmetric stretching mode at 1217 cm<sup>-1</sup>) are observed only above 700 K. As previously reported, these reactions can also occur thermally at these so high temperatures.

The simultaneous analysis of the surface species shows that the activated catalyst transmits a part of the IR radiation (Fig. 12) in the medium frequency region (2000-900 cm<sup>-1</sup>). In the available spectral region a strong band is present centered near 1470 cm<sup>-1</sup> is likely associated to surface carbonates which resist outgassing at 773 K, similar to those observed also on the bare support. Upon ethanol adsorption, a couple of strong bands appear at 1110 and 1060 cm<sup>-1</sup>, with a shoulder at 1165 cm<sup>-1</sup>. This absorption is typical of surface ethoxy groups. By increasing contact temperature above 423 K the sample transmittance suddenly decreases, providing evidence of the reduction of CuO to Cu metal specie, at 473 K. In the meantime, the bands of ethoxy groups modify in the shape, with a single peak at 1116 cm<sup>-1</sup> remaining, possibly associated to ethoxy-groups adsorbed on metallic copper [50]. This band too disappears at higher temperatures.

### 3.4 Characterization of spent catalysts.

In Figure 13, the FE-SEM images of the spent Cu-containing catalysts are shown. They resemble those of the corresponding fresh catalysts. However, the EDX analyses centered on the bright particles show a very high weight concentration in copper, mostly > 85 wt%, with very low oxygen concentrations (< 8%) showing that they are essentially constituted by metallic copper, interacting with a zinc-poor spinel type phase. UV-vis data also confirm reduction of copper to metallic state, showing that the spent catalyst entirely absorb the visible and UV light. Thus, CuO-containing particles interacting with Zn-poor spinel-type particles reduce spontaneously during reaction to copper metal. EDX data also show that carbon present in these particles (5-0.5 wt%, the less the higher Cu content) is comparable or lower than that observed over the fresh catalyst (due to carbonate species), while areas with low Cu content (< 15 %) may have higher C content (15-8 %). This suggests that carbon deposits, if any, form over the bare support or over dispersed copper more than over the copper metal particles. In any case, carbon-rich particles never are observed.

## 4. Discussion

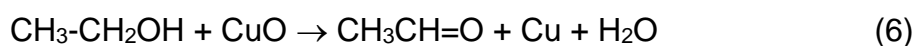
The data reported above show that Cu/ZnAl<sub>2</sub>O<sub>4</sub> catalysts have an excellent activity and selectivity in ethanol dehydrogenation to acetaldehyde. In particular, the three copper-containing catalysts show selectivity to acetaldehyde in excess of 95 % at low conversion (< 50 %) at 523-623 K. This compares well with very selective catalysts reported recently in the literature, such as e.g. supported Gold [13] and Silver [51], Cu/Carbon [52] and highly diluted Ni-Cu nanoparticles [14,15] that show 95-100% selectivity to acetaldehyde at moderate conversions. Over our three catalysts, the only other product observed at low conversion is ethylacetate (< 5 % selectivity) which is potentially a useful product to be obtained by ethanol, which can be easily recovered and valued. We have to mention that our laboratory conditions differ from potential industrial condition not only in terms of time on stream (few hours timescale), but also in terms of ethanol feed concentration (diluted feed). On the other hand, our study confirms that copper-based catalysts, and in particular those arising from the Cu/ZnO/Al<sub>2</sub>O<sub>3</sub> system are competitive with other systems, including some proposed recently [13,14,15], as very selective for the ethanol dehydrogenation process, which were tested under even more diluted conditions than ours.

Additionally, the catalysts studied here show persistence of high selectivity to acetaldehyde (> 90 %) also at near total conversion. The performances we report here are comparable

with those reported previously for a 10 % CuO/ $\gamma$ -Al<sub>2</sub>O<sub>3</sub>/cordierite monolith catalyst [53] and apparently superior to those reported for Cu/mesoporous carbon catalysts [54] and for Cu/ZrO<sub>2</sub> catalysts [55]. The Cu-ZnO-Al<sub>2</sub>O<sub>3</sub> system is also more environmentally friendly than those based on copper chromite, used in the past, due to the absence of chromium that represents a potential danger in the catalyst preparation and successive disposal .

Among the materials investigated here, the Cu30ZA catalysts is the most active giving rise to near 90 % yield to acetaldehyde at 623 and 673 K thus coupling very high activity and very high selectivity at these temperatures. In our conditions, thermodynamic equilibrium for dehydrogenation reaction is nearly fulfilled at 673 K. These performances, obtained with a diluted feed as usual for academic investigations, appear to be very interesting taking into account that most of the alternative catalysts showing very high selectivity at low conversion, usually show a drop in selectivity when conversion becomes very high. Also in these conditions, the predominant byproduct is ethylacetate, a useful compound to be prepared from ethanol.

A similarly high selectivity (95 %) is also observed for the Cu10ZA catalyst, whose activity is, however, definitely lower. These data suggest that the most active sites for the dehydrogenation reactions are associated to the metallic copper nanoparticles, that are present over both Cu10ZA and Cu30ZA but are definitely more abundant on the latter. The data show that the copper oxide nanoparticles present over the fresh catalysts reduce spontaneously during the reaction. These particles seem to grow preferentially over Zn-deficient spinel particles. The IR experiment performed on Cu10ZA provides evidence of the reduction of the catalyst in the 423-473 K range, i.e. at the temperature when conversion in the flow reactor is still very low, if any. In the IR experiment carried out over the Cu10ZA catalyst, acetaldehyde is already observed at 473 K while in the flow reactor significant catalytic activity is only found at 623 K. This unusual difference between the two experiments can be associated to the activation process of the catalysts, we did not pre-reduce before experiments. This activation process consists in the reduction of CuO to Cu metal nanoparticles. The reductant is the same reagent, i.e. ethanol. It is quite reasonable to suppose that the acetaldehyde formed at very low temperature in the IR experiment is due to the stoichiometric process resulting in the reduction of copper



producing also water which is in fact revealed in the gas phase, while only at higher temperatures the true catalytic reaction (1), catalyzed by Cu metal particles, occurs. In any case, it is evident from our data that the catalysts studied here do not need real pretreatments, being activated (or conditioned) spontaneously in the ethanol feed.

As deduced from FE-SEM images, the Cu-rich particles mostly grow over Zn-deficient spinel particles with composition  $Zn_xAl_2O_{3+x}$ , with  $x < 1$ . It is suggested that impregnation / calcination with cupric ions first allows to “saturate” the structure forming stoichiometric spinels with composition  $Cu_{1-x}Zn_xAl_2O_4$ , over which nucleation of CuO is favored. These CuO-rich particles reduce to Cu-rich particles during the reduction/conditioning step. In contrast, on nearly stoichiometric spinel particles, with composition  $\sim ZnAl_2O_4$ , copper tends to disperse homogeneously as a “surface monolayer”. The number of these metallic Cu species interacting with sub-stoichiometric spinel probably decreases when Cu loading increases from Cu10ZA to Cu50ZA, and this is a possible reason for the lower activity of the latter with respect to the former.

Both the flow reactor and the IR experiment show that the acetaldehyde is a primary product of ethanol conversion being likely produced by dehydrogenation/decomposition of the surface ethoxy- groups. The data reported for the Cu10ZA catalyst indicate that a point allowing high selectivity to acetaldehyde is poisoning of the sites active for competitive reactions such as ethanol dehydration to diethyl ether as well as ethylene. On the other hand, acetaldehyde selectivity is limited at high temperature, due to its instability towards decomposition to methane and CO, which is observed also un-catalytically, as well as towards reactions forming acetone and propene.

## 5. Conclusions.

According to the above data, the following conclusions can be drawn:

1. The catalytic system Cu/ZnAl<sub>2</sub>O<sub>4</sub> is very efficient for the dehydrogenation of ethanol to acetaldehyde, with selectivities in excess of 95 % at low conversion, persisting also at total conversion, allowing yields of 90 %.
2. The predominant secondary product at low conversion is ethylacetate, a useful byproduct.
3. The most active species appear to be on copper metal nanoparticles grown over Zn-poor substoichiometric spinel nanoparticles.
4. The catalysts reduce and condition themselves on stream by reacting with ethanol.

5. The selectivity to acetaldehyde decreases at higher temperature ( $> 673$  K) due to overconversion of acetaldehyde to thermodynamically more stable products such as methane, acetone, propene and carbon oxides, as well as to increased competition with the more favoured dehydration reaction to ethylene.
6. IR spectra show the intermediacy of Cu-bonded surface ethoxy- groups.
7. High selectivity of these catalysts to acetaldehyde is also due to the ability of dispersed copper to poison the dehydration activity of Zn aluminate, thus reducing to zero its activity in producing diethyl ether and ethylene at low temperature.

**Acknowledgements.** The collaboration of Michele Pastorino and Antonio Bacigalupo during the preparation of their bachelor's theses, is gratefully acknowledged.

**Figure Captions.**

**Figure 1.** Adsorption isotherms and pore size distribution plots of the fresh samples.

**Figure 2.** XRD patterns of the fresh samples.

**Figure 3.** FE-SEM micrographs of the fresh samples acquired using SE signal.

**Figure 4.** FTIR skeletal spectra (KBr pressed disks) of the fresh catalysts.

**Figure 5.** Diffuse Reflectance UV-Vis spectra of the fresh catalysts .

**Figure 6.** Thermodynamic equilibrium compositions for the different investigated mixtures with the same reaction condition employed in catalytic experiments; a) ethanol/water/acetaldehyde/H<sub>2</sub>, b) ethanol/water /DEE/ethylene, c) ethanol/water /DEE/ethylene/acetaldehyde/H<sub>2</sub>, d) ethanol/water /DEE /ethylene /acetaldehyde /H<sub>2</sub> /propylene/CO<sub>2</sub>.

**Figure 7.** Catalytic activity of ZA support in terms of ethanol conversion and product selectivities as a function of temperature

**Figure 8.** Catalytic activity of Cu10ZA in terms of ethanol conversion and product selectivities as a function of temperature

**Figure 9.** Catalytic activity of Cu30ZA in terms of ethanol conversion and product selectivities as a function of temperature

**Figure 10.** Catalytic activity of Cu50ZA in terms of ethanol conversion and product selectivities as a function of temperature

**Figure 11.** IR experiments of ethanol conversion on Cu10ZA: gas phase spectra in function of the temperature.

**Figure12.** IR experiments of ethanol conversion on Cu10ZA: spectra of the catalyst.

**Figure13.** FESEM micrographs of the spent catalysts.

ACCEPTED MANUSCRIPT

Table 1

Sample	% CuO 100 wt <sub>CuO</sub> /wt <sub>ZnAl<sub>2</sub>O<sub>4</sub></sub> nominal	% Cu (RED)* 100wt <sub>Cu</sub> /wt <sub>C</sub> AT nominal	% Cu from ICP-OES wt <sub>Cu</sub> /wt <sub>CAT</sub>	S <sub>BET</sub> m <sup>2</sup> /g <sub>CAT</sub>	S <sub>BET</sub> m <sup>2</sup> /g <sub>SUP</sub> P	A <sub>SUPP/atCu</sub> * Å <sup>2</sup> nominal	V <sub>POR</sub>	D <sub>POR</sub>
ZA	0	0	-	95	95	--	0.210	6.5
Cu10Z A	10	7.4	7.17	84	92	11.9	0,177	6.5
Cu30Z A	30	19.3	18.51	70	91	3.5	0.154	6.3
Cu50Z A	50	28.5	29.54	60	90	2.4	0.139	6.3

\* Nominal composition data calculated for the reduced catalyst

## References

### References

- [1] K. Musialska, E. Finocchio, I. Sobczak, G. Busca, R Wojcieszak, E. Gaigneaux, M. Ziolek, *Appl. Catal. A: Gen.* 384 (2010) 70–77
- [2] P. Kaminski, M. Ziolek, J.A. van Bokhoven, *RSC Adv.*, 7 (2017) 7801-7819.
- [3] M. Trejda, K. Stawicka, M. Ziolek, *Appl. Catal. B: Envir.* 103 (2011) 404–412
- [4] K. Stawicka, A. E. Díaz-Álvarez, V. Calvino-Casilda, M. Trejda, M.A. Bañares, M. Ziolek, *J. Phys. Chem. C*, 120 (2016) 16699–16711.
- [5] H. Golinskaa, E. Rojas, R. López-Medina, V. Calvino-Casilda, M. Ziolek, M.A. Bañares, M.O. Guerrero-Pérez, *Appl. Catal. A: Gen.* 380 (2010) 95–104
- [6] A. Limayem, S.C. Ricke, *Prog. Energy Combust. Sci.* 38 (2012) 449-467.
- [7] M. Balat, *Energy Convers. Manag.* 52 (2011) 858-875.
- [8] J. Sun, Y. Wang, *ACS Catalysis* 4 (2014) 1078-1090
- [9] M. Eckert, G. Fleischmann, R. Jira, H.M. Bolt, K. Golka, Acetaldehyde, in *Ullman's Encyclopedia of Industrial Chemistry*, Wiley-VCH Verlag GmbH & Co. KGaA, Weinheim (2012).
- [10] Acetaldehyde Market trends, Global Industry Analysts Inc., [strategy.com/MarketResearch/Acetaldehyde-Ethanal-Market-Trends.asp](http://strategy.com/MarketResearch/Acetaldehyde-Ethanal-Market-Trends.asp)
- [11] A. Chauvel, G. Lefebvre, *Petrochemical processes*, 2.. Major oxygenated, chlorinated and nitrated derivatives, Gulf Publishing, Houston, (1989), p. 31-33.
- [12] K. Weissermel, H.-J. Arpe, *Industrial Organic Chemistry* Wiley, 3rd ed., p. 167.
- [13] Y. Guan, E.J.M. Hensen, *Appl. Catal. A: Gen.* 361 (2009) 49–56
- [14] J. Shan, N. Janvelyan, H. Li, J. Liu, T.M. Egle, J. Ye, M.M. Biener, J. Biener, C.M. Friend, M. Flytzani-Stephanopoulos, *Appl. Catal. B: Environ.* 205 (2017) 541–550
- [15] J. Shan, J. Liu, M. Li, S. Lustig, S. Lee, M. Flytzani-Stephanopoulos, *Appl. Catal. B: Environ.* 226 (2018) 534–543
- [16] G. Ertl, H. Knözinger, J. Weitkamp, *Handbook of Heterogeneous Catalysis*, Vol. 5, VCH, Weinheim, Germany, 1997, p. 2140.
- [17] A. Keshavaraja, J.V. Samuel, A.V. Ramaswamy, United States Patent 5723679 (1998) to CSIR, India.
- [18] J.N. Keuler, L. Lorenzen, S. Miachon, *Appl. Catal. A: Gen.* 218 (2001) 171-180.
- [19] Z. Liu, W. Huo, H. Ma, K. Qiao, *Chinese J. Chem. Eng.*, 14 (2006) 676-684.
- [20] G. Busca, *Heterogeneous Catalytic Materials*, Elsevier, Amsterdam, 2014, p. 325.

- [21] K.C. Waugh, *Catal. Lett.* 142 (2012) 1153-1166.
- [22] B. A. Peppley, J. C. Amphlett, L. M. Kearns, R. F. Mann, *Appl. Catal. A: Gen.* 179 (1999) 21-29.
- [23] O. Kumberger, M.J. Sprague, O. Hofstadt, US patent 6051163 (2000) to BASF
- [24] G. J. Kelly, F. King, M. Kett, *Green Chem.* 4 (2002) 392-399.
- [25] Z. Liu, W. Huo, H. Ma, K. Qiao, *Chinese J. Chem. Eng.*, 14 (2006) 676-684.
- [26] T.K. Phung, A. Lagazzo, M.A. Rivero Crespo, V. Sanchez Escribano, G. Busca, *J. Catal.*, 311 (2014) 102-114
- [27] T.K. Phung, L. Proietti Hernandez, A. Lagazzo, G. Busca, *Appl. Catal. A: Gen.*, 493 (2015) 77-89.
- [28] T.K. Phung, R. Radikapratama, G. Garbarino, A. Lagazzo, P. Riani, G. Busca, *Fuel Proc. Tech.*, 137 (2015) 290-297.
- [29] C. Wang, G. Garbarino, L.F. Allard, F. Wilson, G. Busca, M. Flytzani-Staphanopoulos, *ACS Catal.*, 6 (2016) 210-218 .
- [30] G. Garbarino, R. Prasath Parameswari Vijayakumar, P. Riani, E. Finocchio, G. Busca, *Appl. Catal. B: Envir.* 236 (2018) 490-500.
- [31] G. Garbarino, P. Riani, M. Villa García, E. Finocchio, V. Sánchez Escribano, G. Busca, *Reac. Kinet. Mech. Cat.* 124 (2018):503-522
- [32] B. Voss, N.C. Schjødt, J.-D. Grunwaldt, S.I. Andersen, J.M. Woodley, *Appl. Catal. A: Gen.* 402 (2011) 69– 79
- [33] PC Zonetti, J. Celnik, S. Letichevsky, A.B. Gaspar, L.G Appel, *J. Mol. Cat. A, Chem.* 334 (2011) 29-34.
- [34] C. Perdomo Rodrigues, P. Da Costa Zonetti, L.G. Appel, *Chem. Cent. J.* 11 (2017) 30
- [35] E.V. Makshina, M. Dusselier, W. Janssens, J. Degreève, P.A. Jacobs, B.F. Sels, *Chem. Soc. Rev.* 43 (2014) 7917-53.
- [36] J. Vazquez Ochoa, C. Bandinelli, O. Vozniuk, A. Chiaregato, A. Malmusi, C. Recchi, F. Cavani, *Green Chem.* 18 (2016)1653-1663.
- [37] J. Sn, K. Zhu, F. Gao, C. Wang, J. Liu, CHF Peden, Y. Wang, *J. Am. Chem. Soc.* 133 (2011) 11096-11099.
- [38] S.J. Gregg, K.S.W., Sing, *Adsorption Surface Area and Porosity*, (1991) Academic Press London.
- [39] W.B. White, B.A. Deangelis, *Spectrochim. Acta A23* (1967) 985-995.
- [40] S.-F. Wang, G.-Z. Sun, L.-M. Fang, Li Lei, X. Xiang, X.-T. Zu, *Scientific Reports*, 5 (2015) 12849
- [41] A.K. Kushwaha, *Comput. Mat. Sci.* 69 (2013) 505-509.

- [42] M. Zawadzki, W. Staszak, F.E. López-Suárez, M.J. Illán-Gómez, A. Bueno-López, *Appl. Catal. A: Gen.* 371 (2009) 92–98.
- [43] G. Busca, in *Metal Oxide Catalysis*, S. D. Jackson and J.S.J. Hargreaves, eds., Vol. 1, 2009, Wiley-VCH, pp. 95-175.
- [44] L. Debbichi, M.C Marco de Lucas, J.F. Pierson, P. Krüger, *J. Phys. Chem. C* 116 (2012) 10232-10237
- [45] G.T. Anand, L.J. Kennedy, U. Aruldoss, J.J. Vijaya, *J. Mol. Struct.* 1084 (2015) 244–253.
- [46] S.E. Karazanov, P. Ravindran, *J. Am. Ceram. Soc.* 93 (2010) 3335-3341
- [47] Q. Shao, L.-Y. Wang, X.-J. Wang, M.-C. Yang, S.-S. Ge, X.-K. Yang, J.-X. Wang, *Solid State Sci.* 20 (2013) 29-35
- [48] Y. Wang, S. Iany, J. Ghanbaja, Y. Fagot-Revurat, Y.P. Chen, F. Soldera, D. Horwat, F. Mücklich, J.F. Pierson, *Phys. Rev. B* 94 (2016) 245418
- [49] R. Martinez Franco, M. Moliner Marin, C. Franch Martí, A. Kustov, A. Corma Canós, *Appl. Catal. B: Envir.* 127 (2012) 273-280.
- [50] S.C. Street, A.J. Gellmann, *Colloids Surf. A. Physicochem. Eng. Asp.* 105 (1995) 27-34.
- [51] V.L. Sushkevich, I.I. Ivanova, E. Taarning, *ChemCatChem* 5 (2013) 1-8.
- [52] M.V. Morales, E. Asedegbega-Nieto, B. Bachiller-Baeza, A. Guerrero-Ruiz, *Carbon* 102 (2016) 426-436
- [53] S.G. Pouloupoulos, H.P. Grigoropoulou, C.J. Philippopoulos, *Catal. Lett.* 78 (2002) 291-296
- [54] Q.-N. Wang, L. Shi, An-H. Lu, *ChemCatChem* 7 (2015) 2846 – 2852.
- [55] A.G. Sato, D.P. Volanti, D.M. Meira, S. Damyanova, E. Longo, J.M.C. Bueno, *J. Catal.* 307 (2013) 1-17.

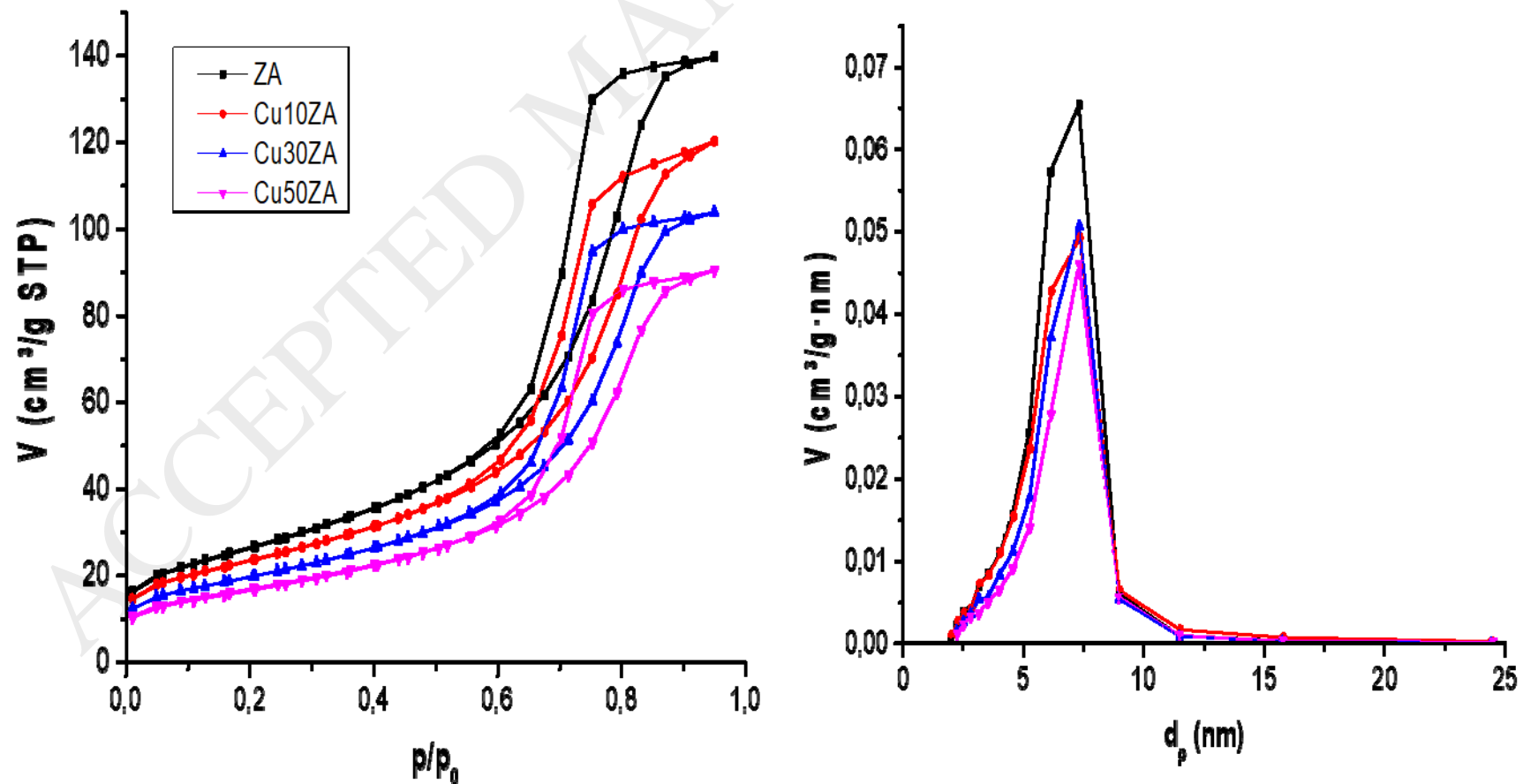


Figure 1

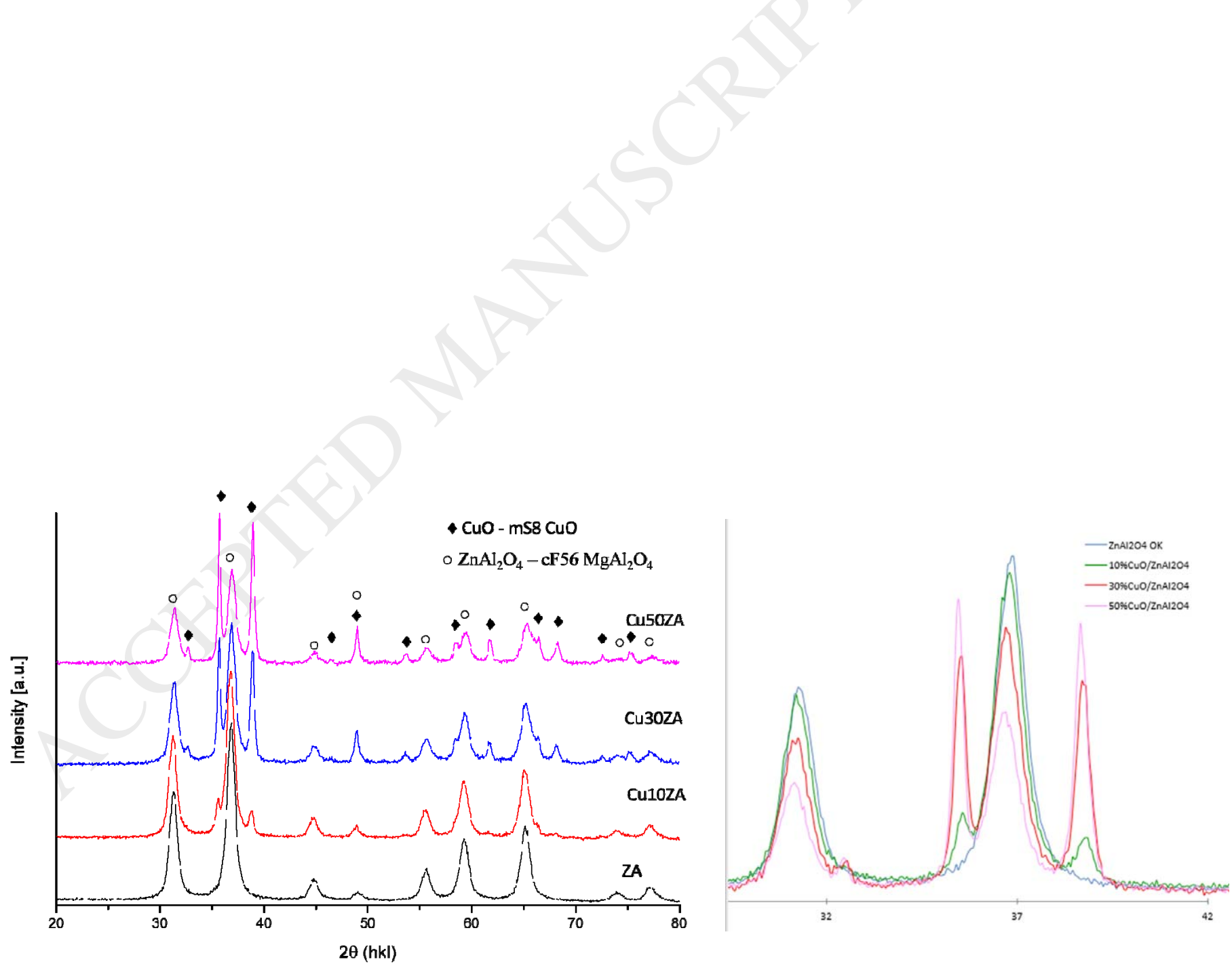


Figure 2

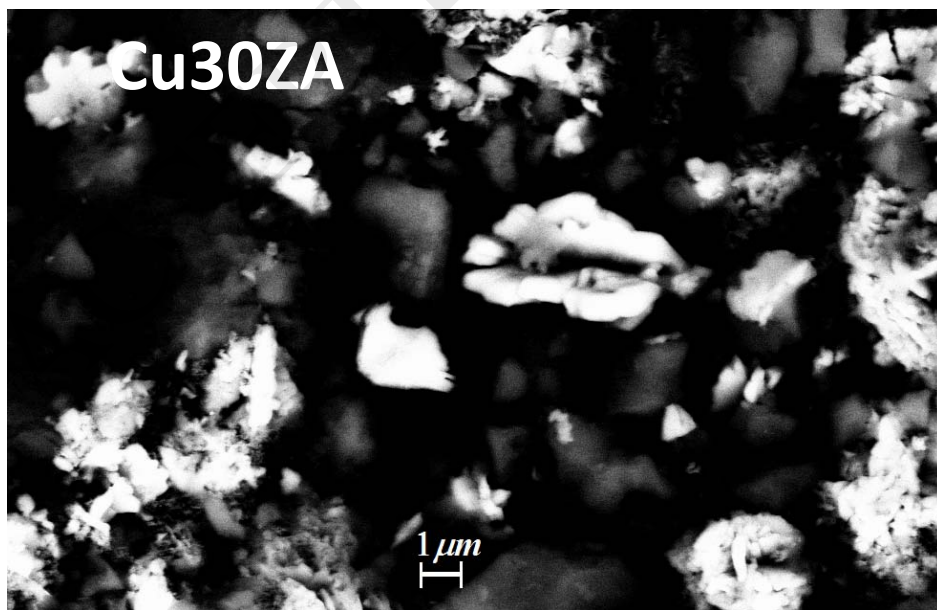
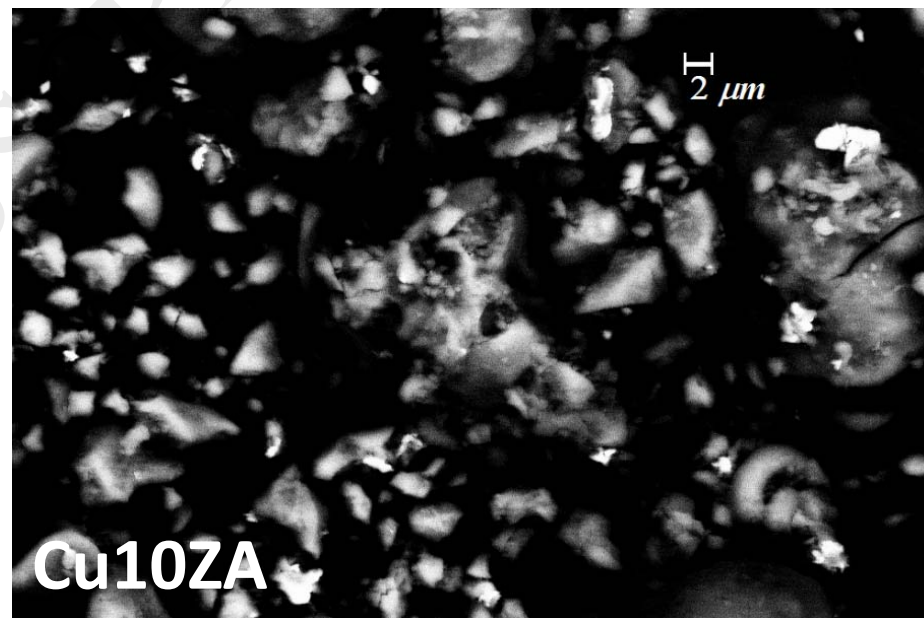
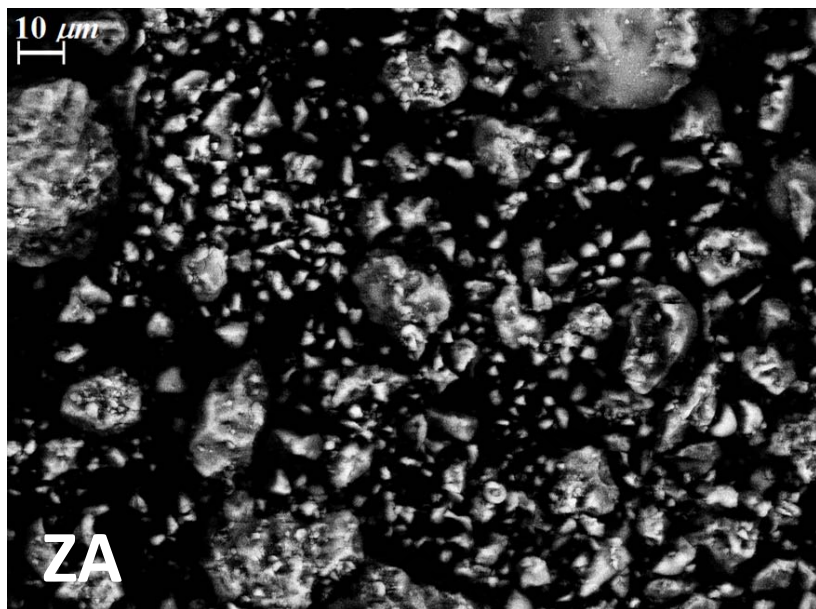


Figure 3

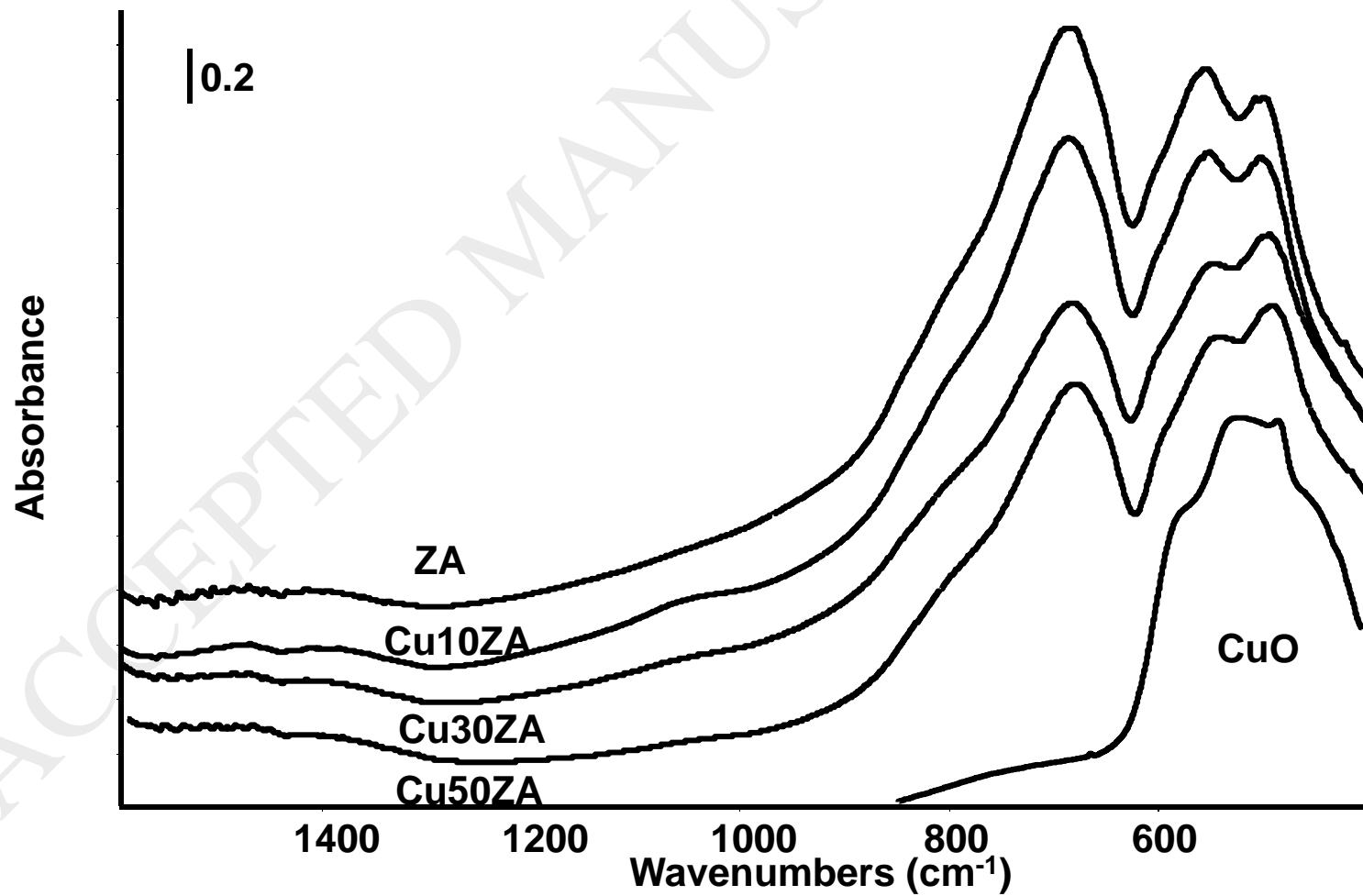


Figure 4

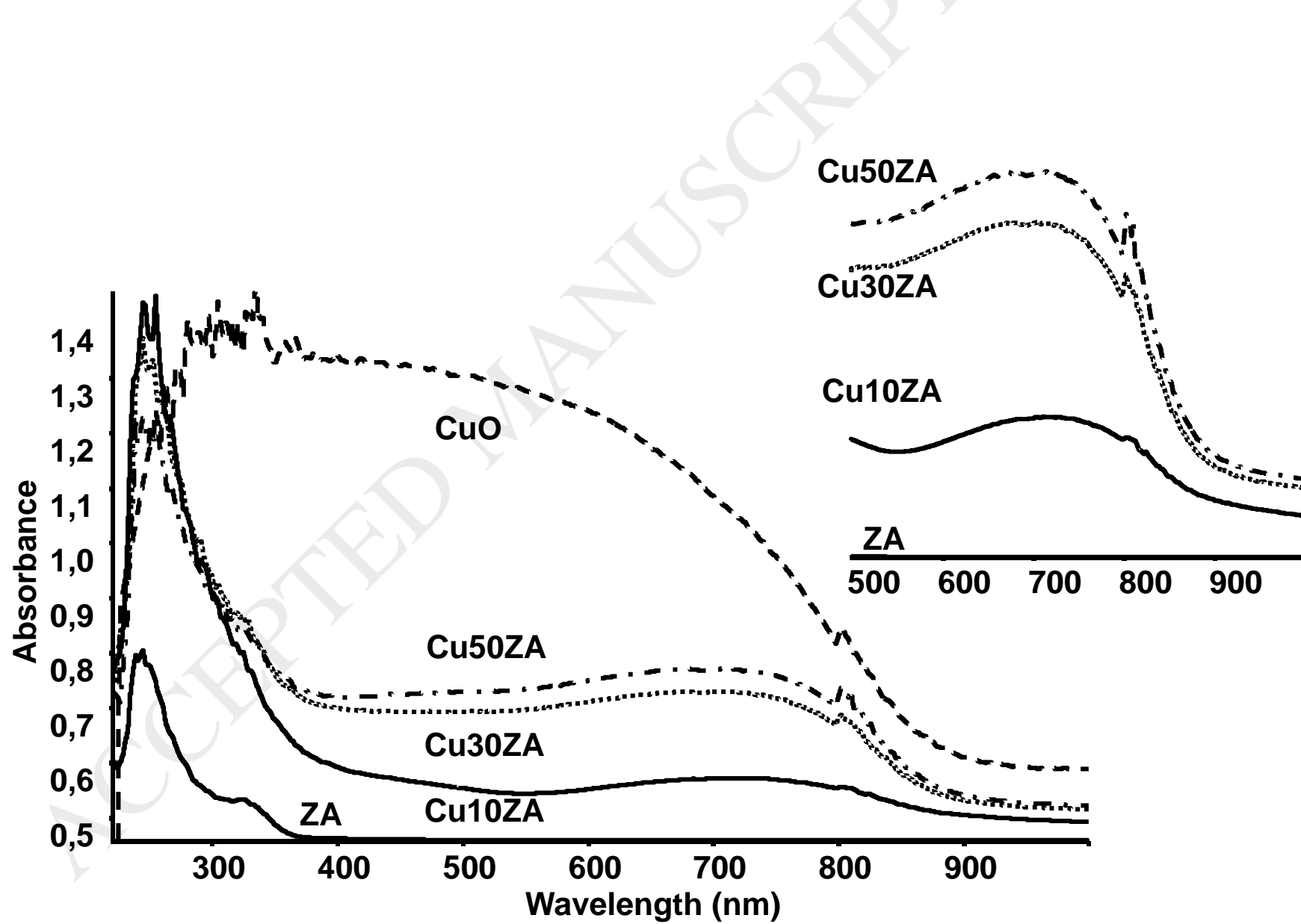


Figure 5

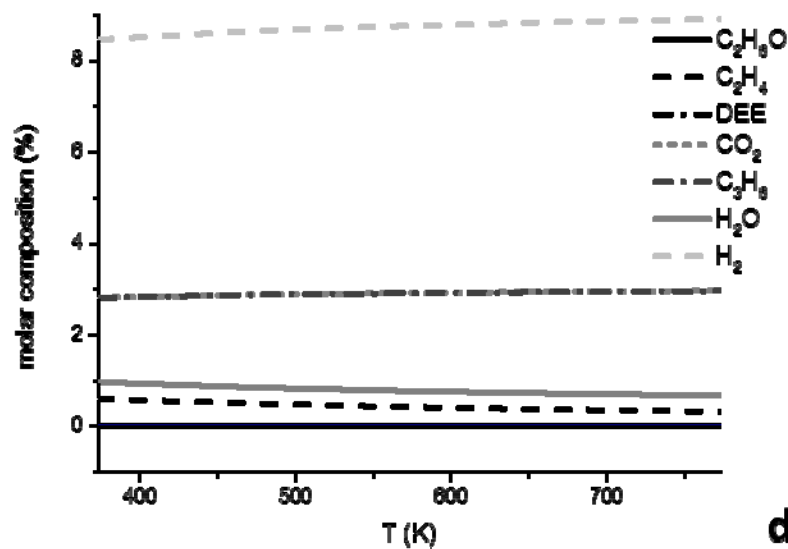
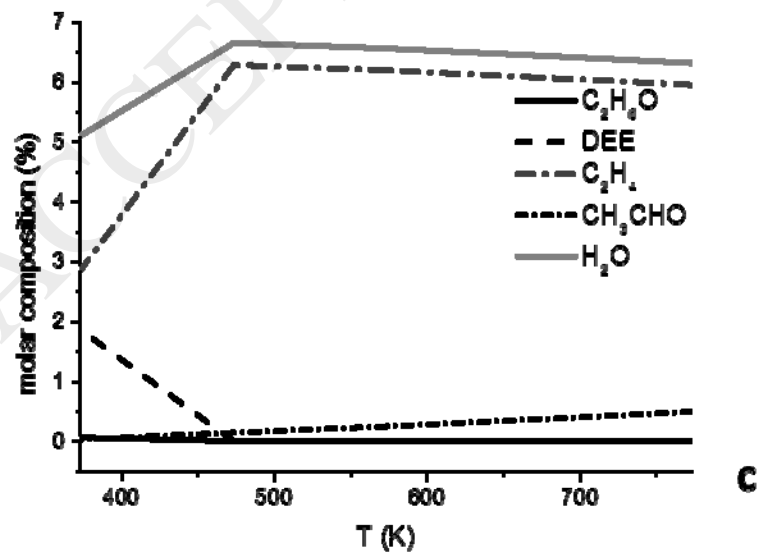
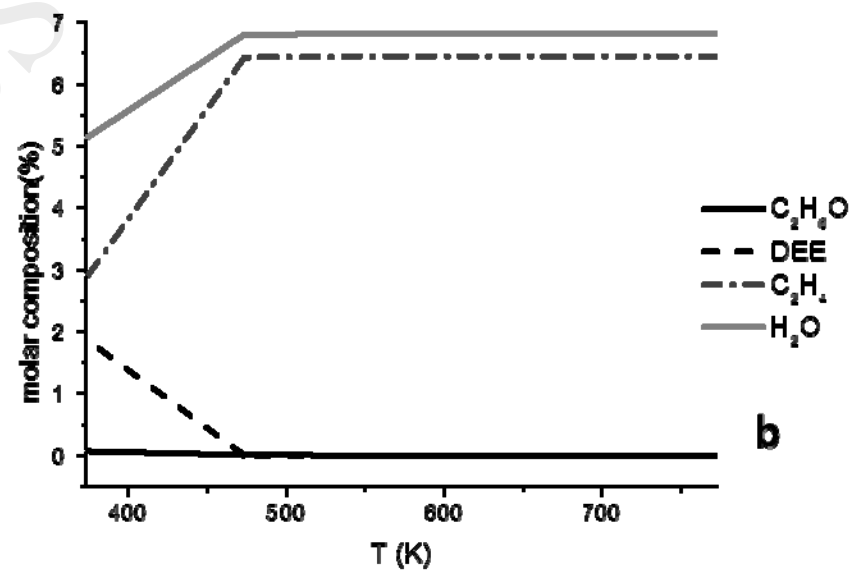
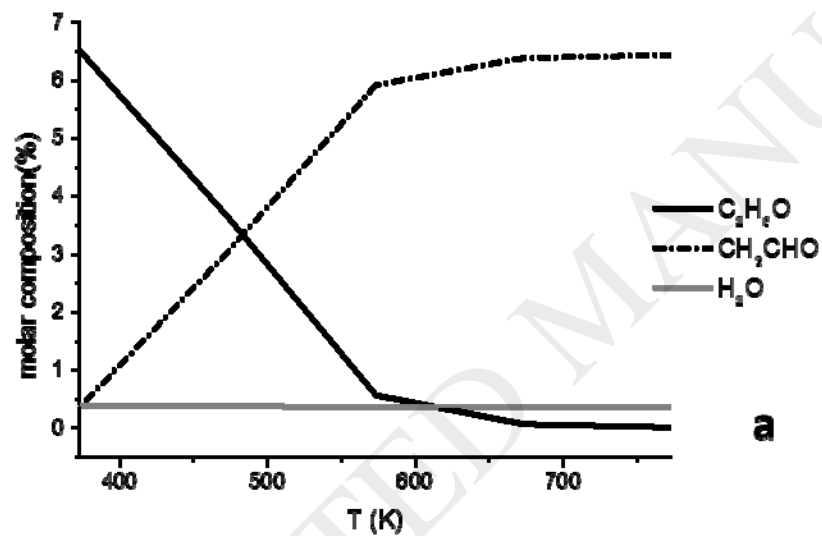


Figure 6

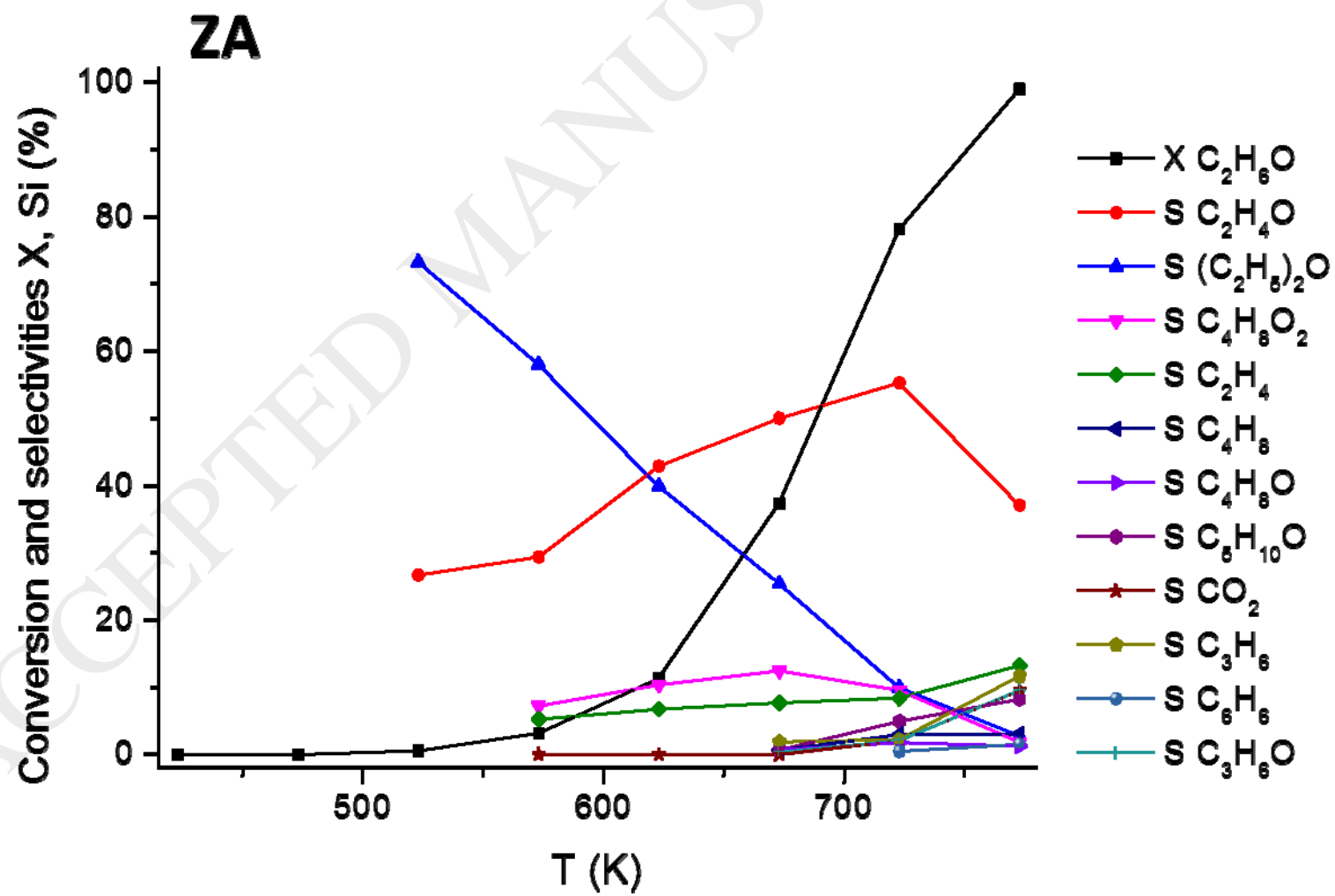


Figure 7

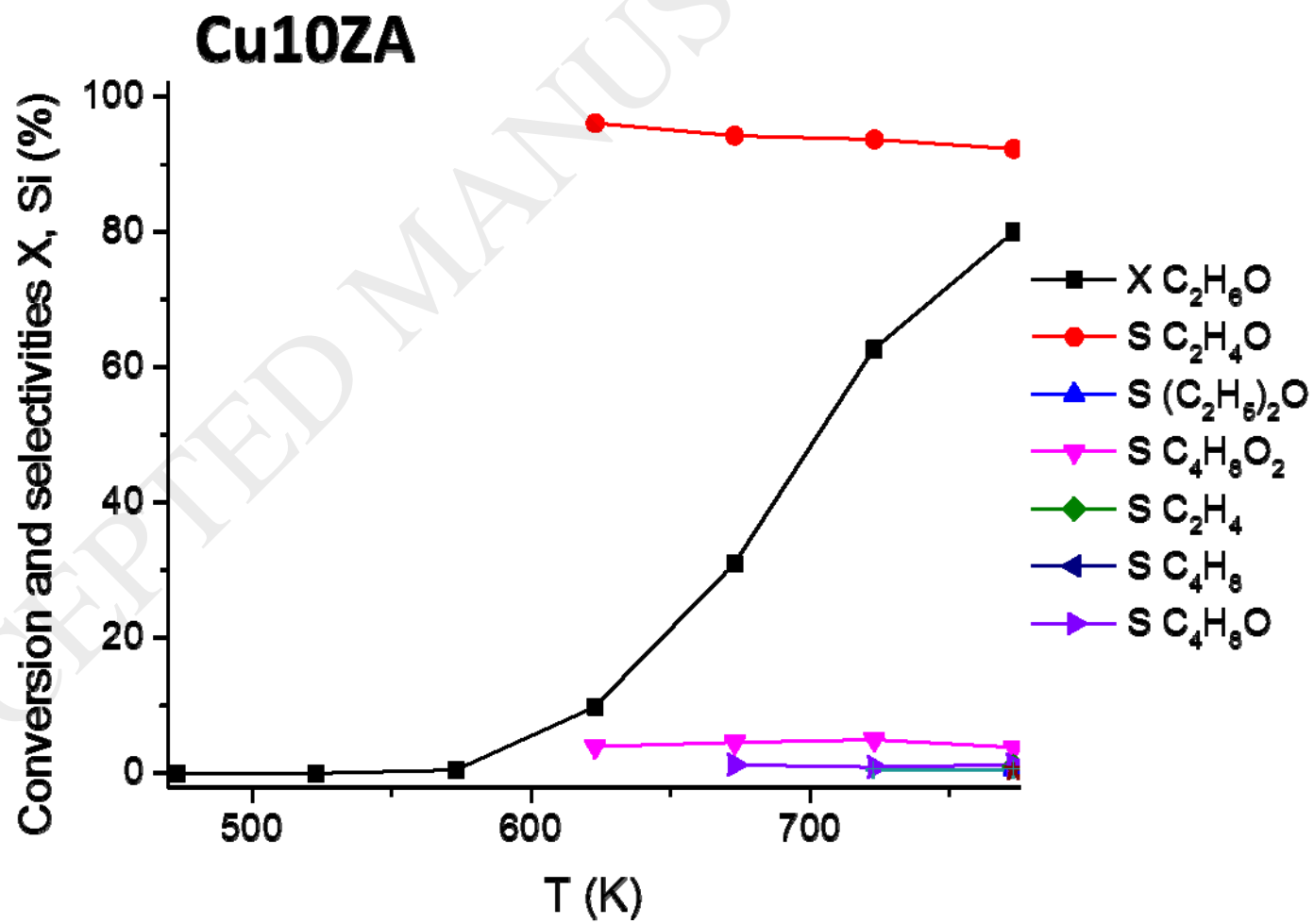


Figure 8

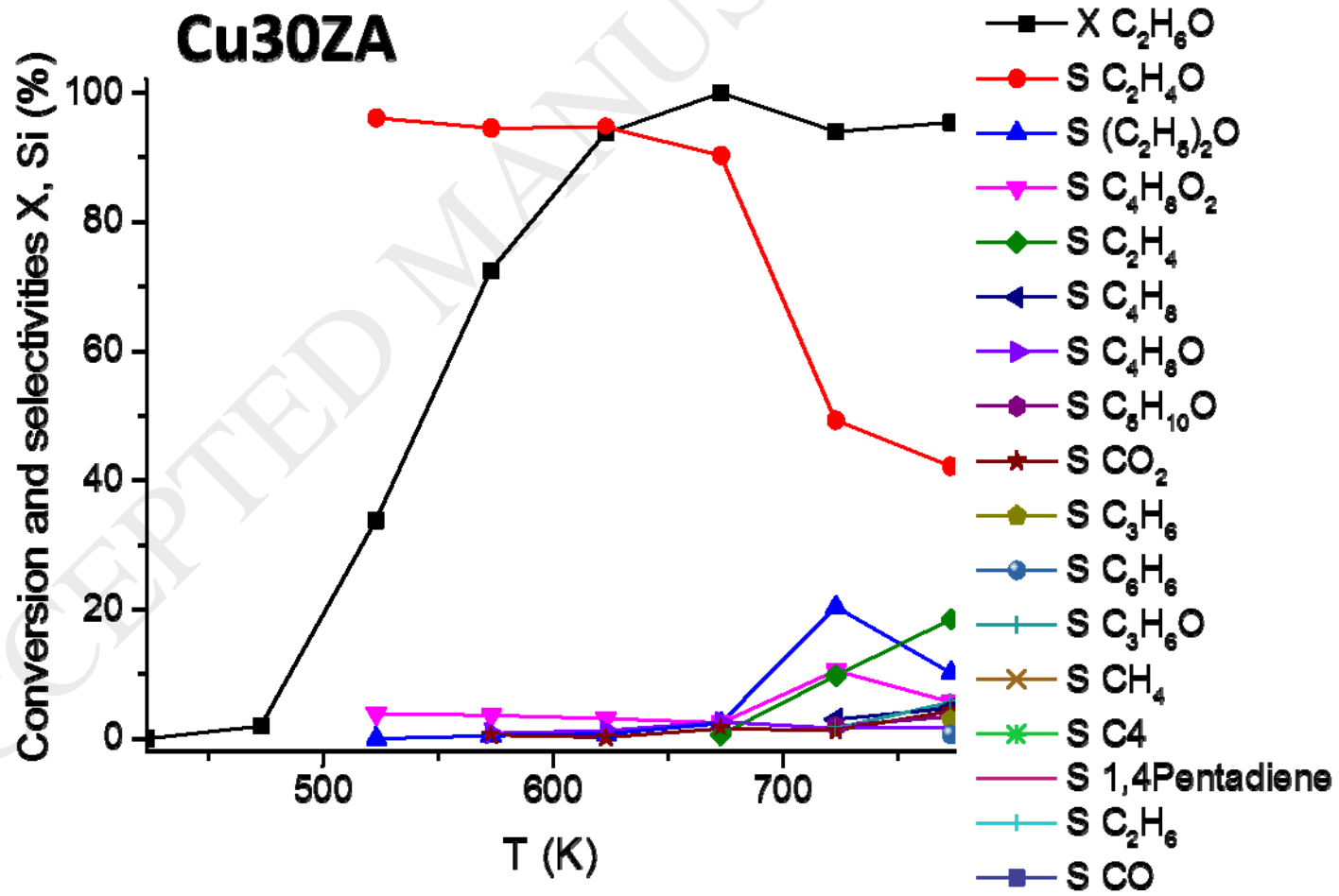


Figure 9

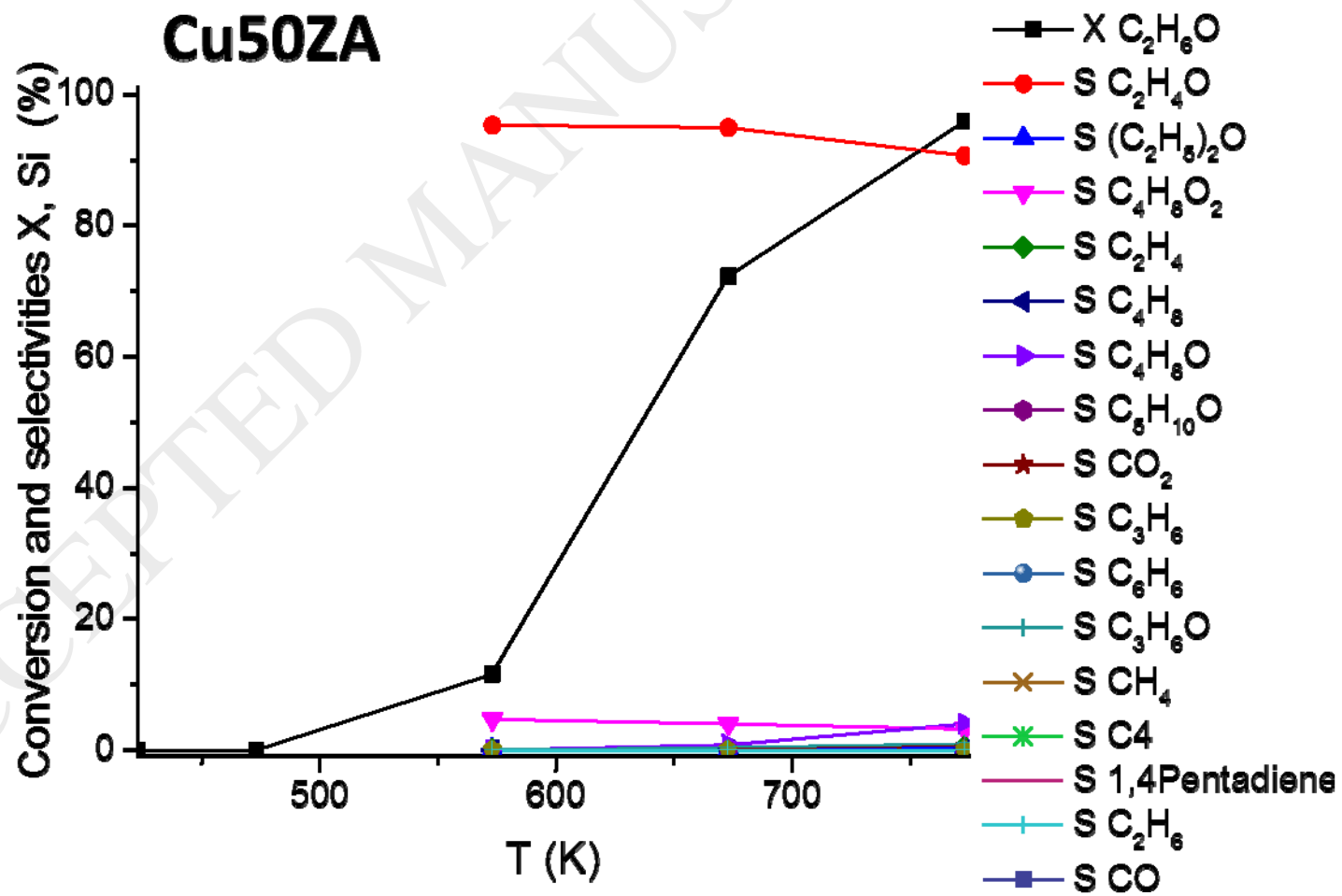


Figure 10

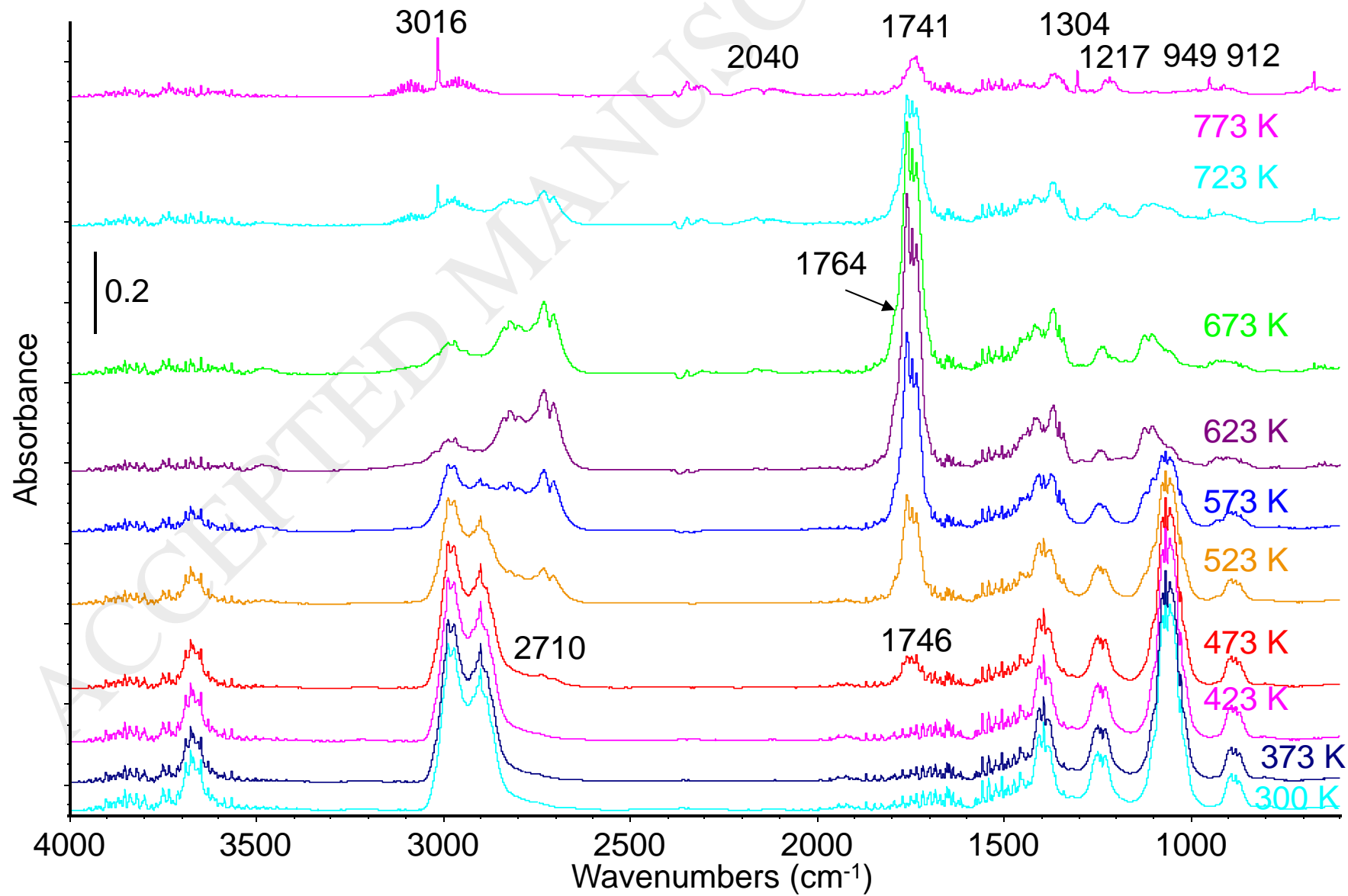


Figure 11

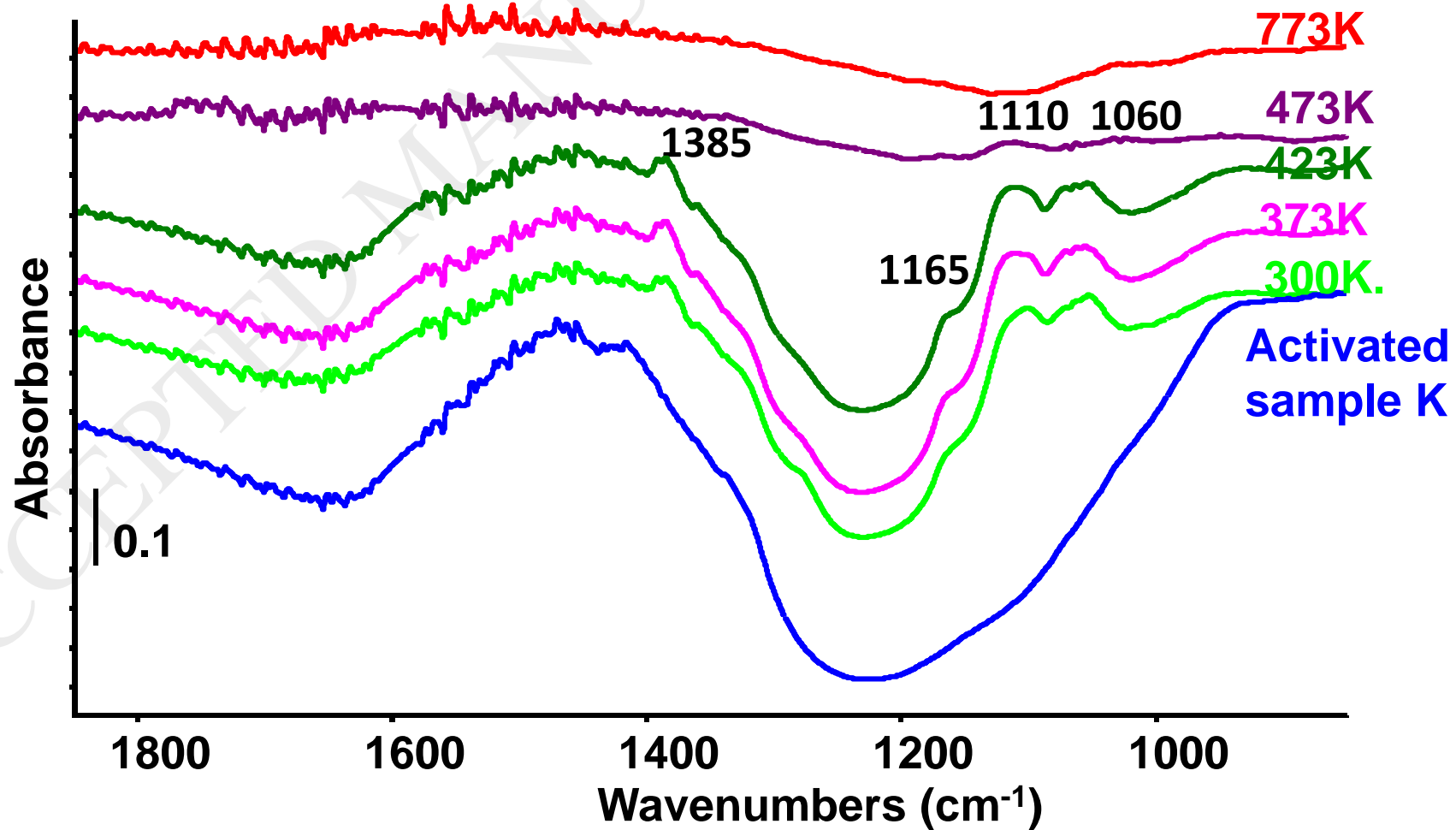


Figure 12

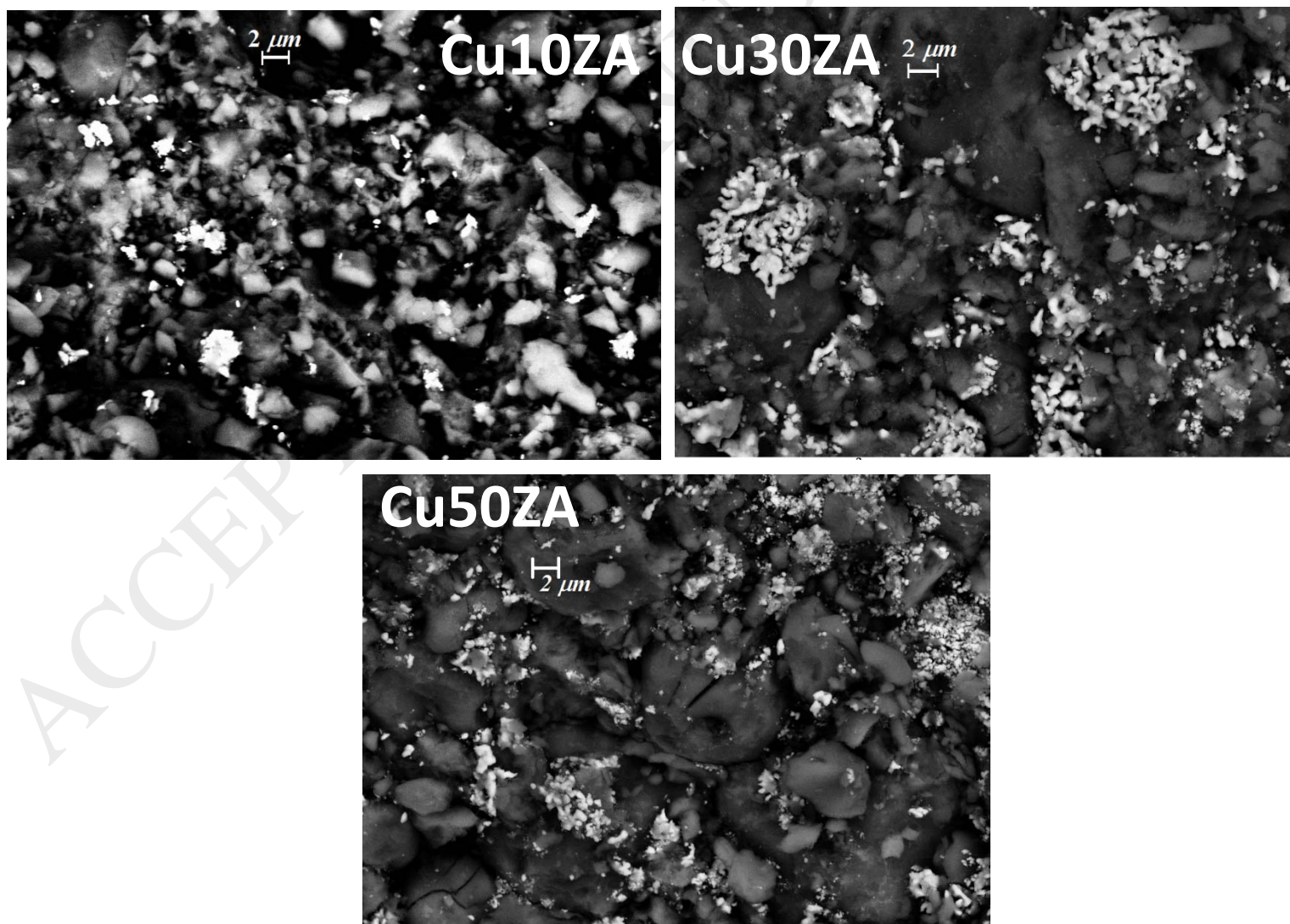


Figure 13